ACS PHYSICAL CHEMISTRY Au
AN OPEN ACCESS JOURNAL OF THE AMERICAN CHEMICAL SOCIETY

Editors' Choice
Open Access

pubs.acs.org/physchemau
Article

Electronic Structure of the S_1 State Manganese Cluster in Photosystem II Investigated Using Q-Band Selective Hole-Burning

Shinya Kosaki, Naohiko Nakamura, Yoshiki Nakajima, Jian-Ren Shen, and Hiroyuki Mino*

Cite This: ACS Phys. Chem Au 2025, 5, 660−671
Read Online

ACCESS | Metrics & More | Article Recommendations | Supporting Information

ABSTRACT: The electronic structure of the S_1 state of photosystem II (PSII) was investigated using selective hole burning of Q-band pulsed electron paramagnetic resonance. The free induction decay and spin−echo signals of the tyrosine radical $Y_D^{\bullet}$ in the plant PSII oscillated because of the magnetic dipole−dipole interaction with the S_1 state Mn cluster. The initial period was 410 ns (2.44 MHz) and was assigned to the $S = 1$ spin state. Based on the oscillation analysis, both Mn1 and Mn4 and both Mn2 and Mn3 were assigned as Mn(III) and Mn(IV), respectively, which is consistent with the quantum chemical calculations. The 410 ns period was accounted for in the simplified model using the isotropic spin density distribution ratio [1.6:−1.1:−1.1:1.6] for Mn1−4 ions. This oscillation was identical with that observed in the presence of methanol. The oscillation decreased in PsbP/Q- and PsbO/P/Q-depleted PSII. In *Thermosynechococcus vulcanus*, two periods, 390 ns (2.56 MHz) and 630 ns (1.59 MHz), were detected, indicating that the cyanobacterial S_1 state includes two isomers, $S = 1$ and $S \geq 2$ spins. The $S \geq 2$ spin was not detected in PsbO/U/V-depleted PSII without polyethylene glycol. The $S \geq 2$ state was consistent with the reported quantum chemical calculation using $S = 3$. A simplified model accounted for the $S = 1$ state as the spin density distribution [1.8:−1.3:−1.3:1.8] and for the $S \geq 2$ state as the isotropic spin density distribution [−0.5:0.5:0.5:0.5] for Mn1−4 ions. In combination with quantum chemical calculations, the most probable protonated structure is W1 = H_2O, W2 = H_2O, O4 = O^{2-}, and O5 = O^{2-} for the S_1 state. These results demonstrate that the selective hole burning method is a powerful tool to complement X-ray studies to determine the valence and protonation structure of manganese clusters, not only in the S_1 state but also in higher S-states and general metal clusters, which would provide important insights into the water oxidation mechanism.

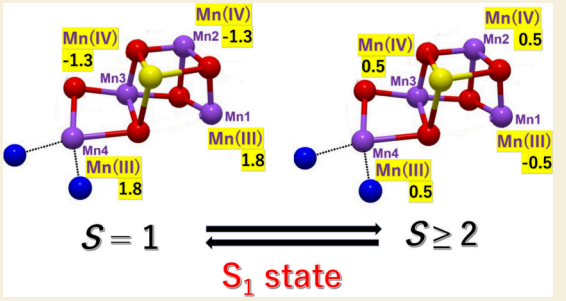

KEYWORDS: *Photosystem II, Oxygen evolution, S_1 state, Mn cluster, EPR, Selective hole-burning*

INTRODUCTION

Photosynthetic oxygen evolution is one of the most important chemical reactions for the maintenance of life on Earth. Molecular oxygen is evolved by a Mn cluster in photosystem II (PSII). The Mn cluster has five different oxidation states, labeled S_0−S_4 in order of redox potential, which cycles through the Kok cycle, and molecular oxygen is spontaneously released during the transition of the S_4−S_0 states (see review in[1−3]). The structure of the Mn cluster was solved using X-ray crystallography at atomic resolution,[4] which showed that the manganese cluster was composed of four manganese atoms (Mn1−Mn4), one calcium atom, and five oxygen atoms serving as oxo-bridges (O1−O5) and were ligated by surrounding amino acid residues (Figure 1). Recent pump−probe X-ray free-electron laser analyses of PSII microcrystals have yielded valuable information on the intermediate state structures during the Kok cycle transitions.[5−9] On the other hand, the mixture of different intermediate states and radiation damage have made experimental evaluation difficult, which are evaluated by model calculations.[10]

However, the protonation state of water and amino acid ligands remains unclear, although some of these have been predicted using quantum mechanical (QM) calculations based on the structures solved (see reviews[3,11−13]).

S_1 is the most stable oxidation state because the lowest oxidation state S_0 is oxidized by the reaction with tyrosine $Y_D^{\bullet}$ in the dark.[14] Thus, the S_1 state is fundamental for elucidating the reaction mechanism. The S_1 state is believed to provide the most reliable structure for X-ray analysis because the higher oxidation S states overlap with the lower oxidation state, and are evaluated using difference Fourier maps between the higher and lower S states.[5−9] However, experimental information on the electronic structure of the S_1 state is extremely limited,[15−20] because it is not readily available from X-ray

Received: July 19, 2025
Revised: August 27, 2025
Accepted: August 29, 2025
Published: September 14, 2025

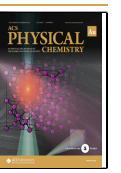

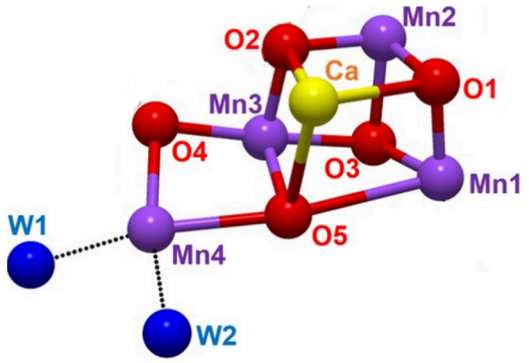

Figure 1. Structure of the water-oxidizing center of photosystem II. The Mn_4CaO_5 cluster and two of the four water ligands (W1 and W2) are shown. The purple, yellow, red, and blue spheres represent Mn, Ca, O, and water oxygen, respectively.

crystallographic structures. Therefore, the boundary conditions for verifying numerous QM calculations have been based mainly on higher oxidation S states, especially the S_2 state, where a famous electron paramagnetic resonance (EPR) signal, multiline signal, is visible.

EPR spectroscopy is a powerful method for investigating the electronic structures of Mn clusters. Since the discovery of the $g = 2$ multiline signal in the S_2 state,[21] this state has been the main target of EPR studies. When studying EPR signals, it is important to connect spin configurations with the spatial molecular structure[11] because the spin wave function does not include spatial coordinates. It is difficult to uniquely assign spin positions to spatial molecular structures. Therefore, model structures based on QM calculations are helpful for understanding the nature of the target molecules. The spin structure and spatial coordinates were mainly linked using the hyperfine analysis of the S_2 state $g = 2$ multiline signal. Ames et al. assigned hyperfine constants to Mn ions in a QM model,[22] where a conversion equation from spin densities to hyperfine constants was applied in the QM calculations. The application of this conversion equation to the Mn cluster is challenging in DFT calculations because it cannot be determined using only one limited structure with one protonation state. Ames et al. proposed a protonated model (W1, W2, O4, O5) = (H_2O, OH^-, O^{2-}, O^{2-}) for S_2 state using DFT calculations.[22] However, recent reports show that W2 = OH^- does not fit the QM/MM model (reviewed in[13]). As water oxidation reactions strongly depend on the location of protons, determining the protonated structure of the manganese cluster is a key factor in elucidating the mechanism.

XRD experiments provide spatial coordinates. In contrast, the electron−electron magnetic dipole interaction (MDI) measurements give rise to distances between electron spins, and the spin wave function is directly linked to the spatial coordinates.[23−26] There are several techniques for detecting MDI, such as pulsed electron−electron double resonance (PELDOR, DEER),[27] selective hole burning,[28−30] and relaxation-induced dipolar modulation enhancement (RIDME).[31] PELDOR is a double-resonance technique that uses two observable EPR signals at different microwave frequencies, and is one of the most popular methods for measuring distances between spins. Currently, PELDOR has many applications, which would be the first choice for general measurements of distances such as radical pairs. The selective hole-burning and RIDME use the relaxation of the off-resonance spin. RIDME is an intermediate technique between the hole-burning and PELDOR methods. In principle, compatible information is obtained from hole-burning, RIDME, and PELDOR. RIDME is effective when the difference in the relaxation times between the two interacting spins is large. However, it is difficult for RIDME to extract nuclear modulation signals overlapping on MDI.[32] The selective hole-burning is detected without nuclear modulation. The detectable range of MDI, i.e. effective distance for detection, is smaller than that of RIDME or PELDOR because it is restricted by the length of the free induction decay (FID) and spin echo. Although these techniques provide almost the same signals, a suitable choice is required depending on the object. The detailed mechanism of hole-burning is reviewed in ref 28.

EPR studies of the S_2 state have shown that it mainly consists of two isomers: a multiline signal state centered at $g = 2$ and a $g = 4$ signal state centered at $g = 4$ in the X-band.[33−35] The hyperfine couplings obtained from the $g = 2$ multiline signal provide a basis for elucidating the electronic structure of the Mn cluster. Isomerization of the S_2 state between $g = 2$ and $g = 4$ is affected by the presence or absence of methanol. The $g = 4$ signal disappears in the presence of methanol.[36] Methanol is one of the closest analogs of water, which also influences the EPR signals in the S_0-S_3 states.[19,37−40] QM calculations have been performed under the assumption that methanol is bound to Mn4.[41] However, no experimental evidence has been found for the direct binding of methanol to the manganese cluster. Alternatively, ENDOR experiments in the S_2 state showed that the methanol molecule is not directly bound to the manganese cluster.[38,39]

QM models have proposed two isomeric structures for the S_2 state: an open-cubane (R-open) and a closed-cubane (L-open).[42,43] The $g = 2$ multiline signal corresponded to the open-cubane structure, and the $g = 4$ signal corresponded to the closed-cubane structure.[42,44] The $g = 4$ signal has been detected in plants and *Chlamydomonas reinhardtii* PSII[45] but not in cyanobacteria.[5−8] In plant and cyanobacterial PSII, the structures immediately surrounding the Mn cluster were almost identical at the amino acid level. The only different amino acid residue is D1-N87; however, this amino acid is irrelevant to S_2 isomerization.[46,47] Therefore, isomerization is caused by extrinsic proteins.[46,47] The three extrinsic proteins were named PsbO/P/Q and PsbO/U/V for plant and cyanobacterial PSII, respectively, among which, PsbO was similar, but the other two proteins were different. The $g = 4$ signal disappeared in the PsbO-depleted PSII, which also lacked the other two extrinsic proteins. For the cyanobacterial PSII, the $g = 4$ signal was undetectable under normal conditions. Another S_2 signal, $g \sim 5$, was also observed as an intermediate, similar to $g = 4$, but with a different spin state and may have structural differences, between plant and cyanobacterial PSII.[46−49]

Although numerous studies have been conducted on the S_2 state, studies on the S_1 state are limited. The S_1 EPR signal is only observable in parallel-polarized EPR.[15−20,50] A weak X-band EPR S_1 state signal was detected in plant PSII at approximately $g = 4.9$. This signal arose from a weakly excited $S = 1$ spin state.[15,19,20] The measurements using the oriented PSII membrane show that the zero-field parameters were $|D| = 0.14\ cm^{-1}$, $|E/D| = 0.11$, and the D-axis was along the membrane plane.[20] The S_1 signal disappeared in the presence of MeOH.[19] Additionally, a different type of S_1 signal with a

https://doi.org/10.1021/acsphyschemau.5c00068
ACS Phys. Chem Au 2025, 5, 660−671

multiline structure has been detected in cyanobacterial PSII.[16−18,50] The signal was assigned to the $S = 2$ or $S = 3$ ground state.[50] The spin distribution can be explained using equivalent hyperfine constants of the four Mn ions.[50] The $S \geq 2$ S_1 signal was also detected in PsbP/Q-depleted plant PSII.[50]

The stable radical $Y_D^\bullet$ is a landmark for the EPR studies of PSII. The structure of the Mn cluster can be directly mapped onto the crystal structure using the magnetic dipole interaction (MDI) between the $Y_D^\bullet$ radical and manganese cluster.[24,25] In the S_0 and S_2 states, the MDI between $Y_D^\bullet$ and $g = 2$ multiline was detected using PELDOR.[23,24] The dipole interactions are 1.2 MHz (850 ns) and 2.4 MHz (420 ns) for S_0[26] and S_2 states.[24] The difference between $Y_D^\bullet$-S_0 state ($S = 1/2$) and $Y_D^\bullet$-S_2 state ($S = 1/2$) is ascribed to different spin distributions of S_0 and S_2 states. Using the crystal structural coordinates and MDI, the spin density distributions on the manganese cluster can be obtained.

On the other hand, it is impossible to apply the PELDOR technique to the S_1 state, as this state cannot be detected using conventional EPR. Alternatively, selective hole-burning can be used to detect the interaction between $Y_D^\bullet$ and the S_1 state manganese cluster. In early experiments, Kodera et al. succeeded in detecting the S_1 state in X-band selective hole-burning,[51] where the distance between the $Y_D^\bullet$ and the manganese cluster was evaluated to be 30 Å. These methodologies should be improved and reevaluated using fine-crystal structural coordinates.

Since the early report,[51] EPR equipment has been improved: (1) The signal resolution has been improved, which enables the detection of small modulations relative to FID amplitude. (2) A stable, commercial Q-band pulsed EPR system has been developed. (3) An arbitrary waveform generator unit (AWG) was installed, which enables microwave phase to be controlled at a high precision. In this study, we applied a selective hole-burning technique to the S_1 state using this improved, Q-band pulsed EPR and evaluated its electronic structure.

MATERIALS AND METHODS

Plant PSII membranes were prepared from spinach as previously described[44] and resuspended in buffer A containing 400 mM sucrose, 20 mM NaCl, and 20 mM MES/NaOH (pH 6.5) (untreated PSII). Methanol (3%) was then added to the final buffer (+MeOH sample). In order to populate the samples to the S_1 state, the samples were incubated at 273 K for 2 h after preillumination.[14] For Mn-depleted spinach PSII, 1 mM NH_2OH was added, incubated for 1 min at 1 mg Chl/mL PSII membranes, and resuspended in buffer A containing 50 mM disodium dihydrogen ethylenediaminetetraacetic acid dihydrate (EDTA·2Na).[52] These samples were inserted into a 1.6 mm quartz EPR tube after centrifugation at 35,000 × g for 30 min.

Thermosynechococcusvulcanus PSII core dimer was prepared as described previously.[53] The sample was resuspended in buffer A containing 10% polyethylene glycol (PEG) 6000, centrifuged at 35,000 × *g* for 30 min, and inserted into a 1.6 mm quartz EPR tube.[47] In order to populate the samples to the S_1 state, the samples were incubated at 293 K (room temperature) for 2 h after preillumination.[6] For Mn depletion, 1 mM NH_2OH was added and incubated for 1 min at 1 mg Chl/mL PSII core and resuspended in buffer A containing 10% PEG 6000 and 50 mM EDTA·2Na. These samples were inserted into a 1.6 mm quartz EPR tube after centrifugation at 35,000 × *g* for 30 min and frozen in liquid nitrogen.

The extrinsic proteins, PsbP/Q, in spinach PSII was depleted by treatment with 2 M NaCl.[47,54] Depletion of PsbO/P/Q in spinach and PsbO/V/U in *T. vulcanus* was performed using 1 M $CaCl_2$ treatment.[47,55] The *T. vulcanus* samples were washed twice with Amicon ultra (100k) for PEG extraction. The Q-band sample tubes were inserted into 5 mm quartz EPR tubes for X-band CW measurements.

For X-band CW EPR measurements, a Bruker EMX spectrometer with a resonator (ER 4122SHQ, Bruker, DE) and a gas flow temperature control system (ESR900, Oxford Instruments, Oxford, GB) were used.

For pulsed EPR measurements, a Bruker E680 spectrometer with a resonator (EN5107D2, Bruker, DE) and a gas flow temperature control system (ESR900, Oxford Instruments, Oxford, GB) were used. The microwave power and pulse phase were controlled using an arbitrary waveform generator unit. The pulse sequence P0 − T − P1 − τ − P2 − τ was used for hole-burning measurements (illustrated in Figure 2). The pulse lengths were set to 1000 (π), 28 ($\pi/2$), and 28 ($\pi/2$) ns for pulses P0, P1, and P2, respectively. The intervals T and τ were set to 14 μs and 1200 ns, respectively. The microwave phases were set to $x - x - y$ for P0 − P1 − P2 pulses. The unwanted signals were removed during the phase cycle. The deadtime was adjusted by comparison with the location of spin echo and around symmetrical signals. In this sequence, the soft pulse P0 creates a hole in the spin A spectrum, and the hole diffuses in the spin A owing to its interaction with the nonresonant spin B.[28] The diffused spin packets were detected as FID after the P1 pulse and as a spin echo after the P2 pulse. The hole trace was obtained by subtracting the signal obtained in the absence of P0 (Figure 2).

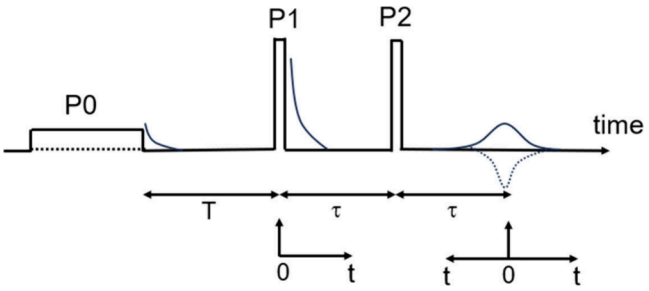

Figure 2. Pulse sequence for the selective hole-burning method. The soft pulse P0 created a selective hole in the EPR spectrum. Spectral diffusion due to spin interaction produces FID after the hard pulse P1 and spin echo after the hard pulse P2. The dashed line shows the pattern when the P0 pulse was turned off. A selective hole-burning trace was obtained by subtracting the P0 pulse on and off.

RESULTS

Figure 3 shows that field swept spectra of (A) X-band CW- and (B) Q-band pulsed EPR of (a) spinach PSII in the presence of 3% methanol, (b) untreated spinach PSII, (c) Mn-depleted spinach PSII, (d) untreated *T. vulcanus* PSII, and (e) Mn-depleted *T. vulcanus* PSII. Background signals for cavity and spike noise were subtracted for (B). The peaks around 11,900 G were artifact arose from subtraction of the background. No S_2 signal was detected in the spectra. Selective hole-burning experiments have been performed at the position of (B) array.

Figure 4 shows the selective hole-burning traces of the untreated plant PSII in the presence of (a) P0 pulse (P0-on) and the absence of (b) P0 pulse (P0-off). The magnetic field was set to $Y_D^\bullet$.

The signal was evaluated by (c) subtracting (a)−(b). Some oscillations were detected in the FID and spin echo, which were ascribed to the MDI between $Y_D^\bullet$ and the Mn cluster.

Selective hole-burning traces were measured in some of the treated PSII samples. These traces are shown in (Figure S1) spinach PSII in the presence of 3% methanol, (Figure S2) *T. vulcanus* PSII, (Figure S3) Mn-depleted spinach PSII, and (Figure S4) Mn-depleted *T. vulcanus* PSII. Figure 5 shows

https://doi.org/10.1021/acsphyschemau.5c00068
ACS Phys. Chem Au 2025, 5, 660−671

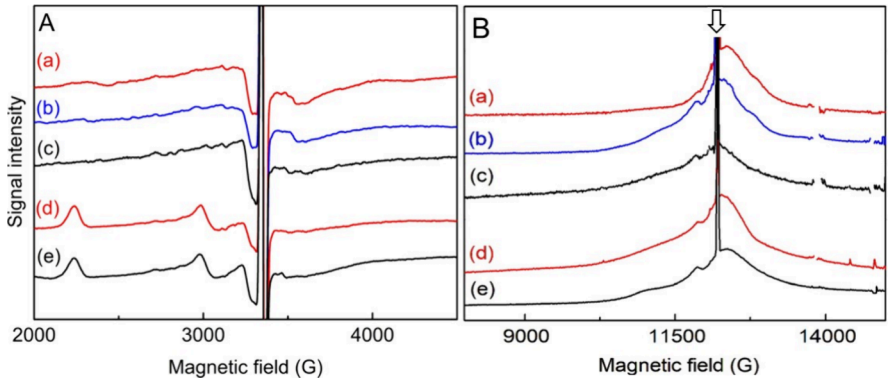

Figure 3. Field swept (A) X-band CW- and (B) Q-band pulsed EPR spectra of (a) spinach PSII in the presence of 3% methanol; (b) untreated spinach PSII; (c) Mn-depleted spinach PSII; (d) untreated *T. vulcanus* PSII; and (e) Mn-depleted *T. vulcanus* PSII. (B) Background signals for cavity and spike noise were subtracted. Experimental conditions: (A) microwave frequency, 9.41 GHz; microwave power, 0.6 mW; modulation amplitude, 20 G; temperature, 6 K; (B) microwave frequency, 34.33 GHz; pulse sequence, $\pi/2$-τ-π; pulse length, 28 ns; interval τ between the mw pulses, 300 ns; repetition time, 100 μs; temperature, 6 K.

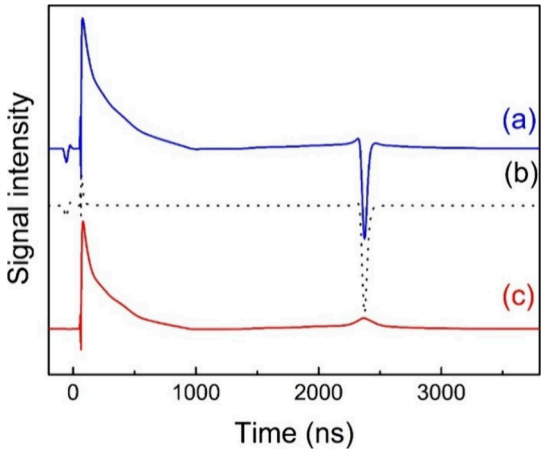

Figure 4. Hole-burning traces of the untreated plant S_1 state PSII with (a) P0 pulse (P0-on) and without (b) P0 pulse (P0-off). Trace (c) was subtracted (P0-off) from (P0-on). Measurement conditions: microwave frequency, 34.2 GHz; magnetic field, 12213 G; pulse length, 1000 ns for P0, 28 ns for P1, 28 ns for P2; duration, 14 μs for T, 1200 ns for τ; repetition time, 5 ms; temperature, 6 K.

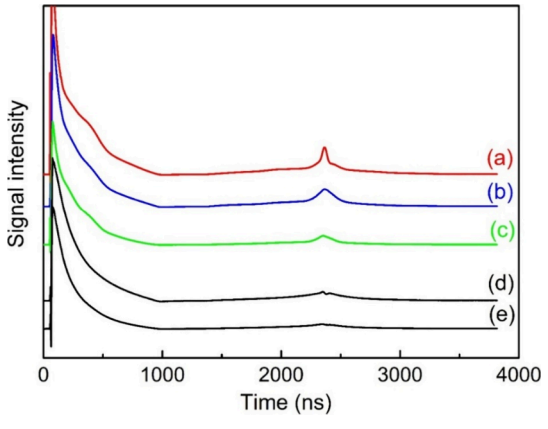

Figure 5. Hole-burning traces of (a) spinach PSII in the presence of 3% methanol; (b) untreated spinach PSII; (c) untreated *T. vulcanus* PSII; (d) Mn-depleted spinach PSII; and (e) Mn-depleted *T. vulcanus* PSII. The traces were obtained by subtracting the P0-off from P0-on traces. The measurement conditions were the same as those shown in Figure 4.

traces of (a) spinach PSII in the presence of 3% methanol, (b) untreated spinach PSII, (c) *T. vulcanus* PSII, (d) Mn-depleted spinach PSII, and (e) Mn-depleted *T. vulcanus* PSII. The oscillation depth and amplitude gradually decreased over time. The oscillation pattern was slightly modified in the *T. vulcanus* PSII. In Mn-depleted PSII, there was no oscillation in the FID or spin echo in both spinach and *T. vulcanus* PSII.

Figure 6 shows the S_1 state traces of (a) spinach PSII + MeOH, (b) untreated spinach PSII, and (c) untreated

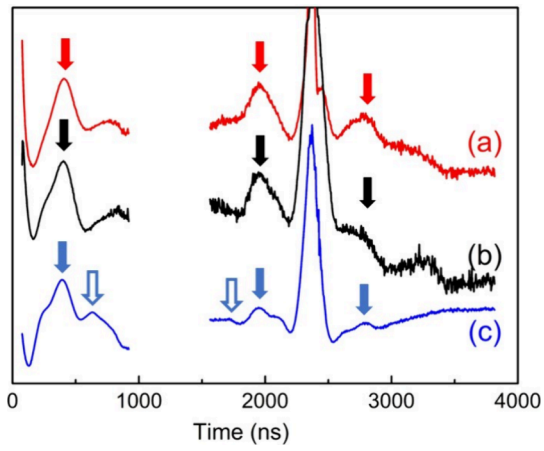

Figure 6. Selective hole-burning traces in the S_1 state of (a) spinach PSII + MeOH, (b) untreated spinach PSII, and (c) untreated *T. vulcanus* PSII. These traces were obtained by dividing the corresponding Mn-depleted PSII. The measurement conditions were the same as those shown in Figure 4. The filled arrays exhibited a peak at approximately 400 ns, ascribed to $\boldsymbol{S} = 1$, and the blank arrays exhibited a peak at 630 ns, ascribed to $\boldsymbol{S} \geq 2$. See text for details.

T. vulcanus PSII, which were obtained by dividing them by the corresponding traces of Mn-depleted PSII. The traces around the P1 and P2 pulses (Figure 2) were removed. The largest periods were detected at approximately 400 ns for all samples. The traces of the untreated and +MeOH spinach PSII were similar, indicating that the S_1 spin state was insensitive to the addition of methanol. Notably, the S_1 signal was not detected in the +MeOH spinach PSII using parallel-polarization EPR. An additional peak at 630 ns was detected in

https://doi.org/10.1021/acsphyschemau.5c00068
ACS Phys. Chem Au 2025, 5, 660−671

T. vulcanus PSII. Other shoulders/peaks at 256 ns are detected in traces (b) and (c).

Figure 7(A) shows the selective hole-burning traces of the (a) untreated, (b) PsbP/Q-, and (c) PsbO/P/Q-depleted

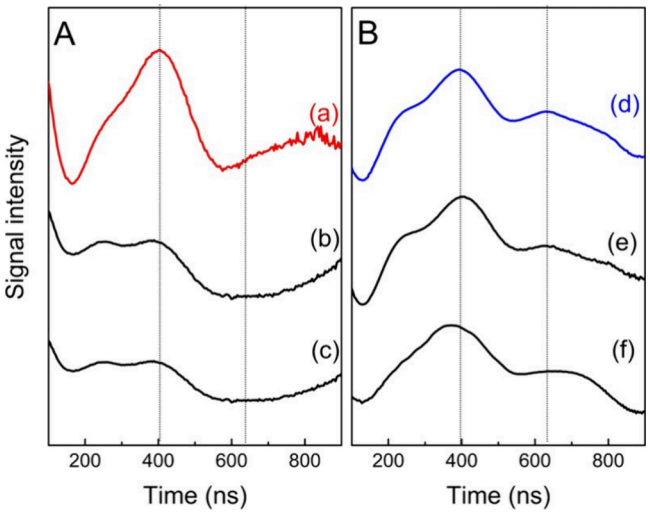

Figure 7. Selective hole-burning traces in the S_1 state of (A) spinach and (B) *T. vulcanus* PSII. The traces were (a, d) untreated, (b) PsbP/Q-depleted, (c) PsbO/P/Q-depleted, (e) PsbO/U/V-depleted PSII in the presence of PEG, and (f) PsbO/U/V-depleted PSII in the absence of PEG. Traces were obtained by dividing those of the corresponding Mn-depleted PSII. The measurement conditions were the same as those shown in Figure 3. Dotted lines indicate 410 (or 390) ns and 630 ns, corresponding to $\boldsymbol{S} = 1$ and $\boldsymbol{S} \geq 2$ spins, respectively. See text for details.

spinach PSII. The first period of 410 ns was decreased in (b) PsbP/Q- and (c) PsbO/P/Q-depleted spinach PSII, and a period of 630 ns was not detected in (b) PsbP/Q- and (c) PsbO/P/Q-depleted spinach PSII. Figure 7(B) shows traces of (d) untreated, (e) PsbO/U/V-depleted *T. vulcanus* PSII in the presence of PEG, and (f) PsbO/U/V-depleted *T. vulcanus* PSII in the absence of PEG. Traces (d) and (e) were similar, but the first period (390 ns) was slightly shifted. Trace (f) had its first peak at 370 ns, and the second period at 630 ns was not detected.

DISCUSSION

Q-band selective hole burning detected a magnetic interaction between the $Y_D^\bullet$ and the S_1 state Mn cluster in both spinach and *T. vulcanus* PSII. Signals were observed for both untreated and + MeOH spinach PSII. A period of approximately 400 ns was observed for all S_1 state traces. In the early report, these modulations were not detected.[51] The main reason for the difference is the improvement of instruments as described above. The previous signal was obtained by dividing signals with different T values. The procedure is reliable for obtaining initial slope of the signals, and therefore reasonable distance was estimated.[51] However, the difference between the signals with different T is small, and includes background signals. In the present work, the signals were obtained by dividing signals in the Mn-depleted PSII under fixing T value.

The 400 ns signal in the untreated spinach PSII can be ascribed to a spin state related to the parallel polarization EPR,[15,19] i.e. weakly excited $\boldsymbol{S} = 1$ spin state. However, the signals were observed for + MeOH spinach PSII. This is in contrast to the previously reported loss of the parallel-polarized S_1 state signal in the presence of methanol in spinach PSII reported previously.[19] Analogous to isomerization in the S_2 state, methanol was expected to exhibit a similar effect on the isomeric equilibrium of the S_1 state. However, the present results indicate that the S_1 state exhibits the same spin state in the presence of methanol. The disappearance of the parallel-polarization S_1 state signal can be ascribed to a small modification in structural symmetry. The parallel-polarization EPR signal is highly sensitive to the zero-field splitting parameters D and E. Particularly, the rhombic parameter E/D is directly related to the spin-transition probability. For the S_1 signal, the small E/D parameter was estimated to be ± 0.11.[20] Because methanol appears to be located proximate to the Mn cluster,[19,39] it may modify the crystalline field of the Mn cluster. If the rhombic parameter E/D decreases (i.e., close to octahedral symmetry), the signal may become undetectable without major modifications to the spin structure.

Different types of EPR signals for the manganese cluster have been reported, which are called 'split signal'.[56−61] The origin of these signals is generally believed to be due to the interaction between $Y_Z^\bullet$ and the manganese clusters. It was reported that the split signal generated by illuminating the S_1 state disappears in the presence of methanol.[58,60] This was interpreted as being due to the weakening of the 'split signal', caused by the upshift of the excited level ($\boldsymbol{S} = 1$) of the S_1 state, and the S_1 state is populated to the ground state ($\boldsymbol{S} = 0$) in the presence of methanol. However, the present work shows that the spin state of S_1 remains in the $\boldsymbol{S} = 1$ spin state even after methanol addition at 6 K. Therefore, methanol is considered to influence not the spin state of the S_1 state, but the exchange interaction between $Y_Z^\bullet$ and S_1 state.

Parallel polarization experiments showed that the S_1 state in the untreated PSII had a ground state with $\boldsymbol{S} = 0$ and a 2.5 K higher excited state with $\boldsymbol{S} = 1$.[19] Because the ground state $\boldsymbol{S} = 0$ does not interact with $Y_D^\bullet$, the MDI is ascribed to the $\boldsymbol{S} = 1$ excited state. In the S_1 state of untreated PSII, the two states, $\boldsymbol{S} = 0$ ground state and $\boldsymbol{S} = 1$ excited state, are considered to populate almost equally at 6 K. Therefore, the detectable population for MDI is half of the reaction centers. In contrast, the modulation depth of the hole-burning signal in the presence of methanol was not decreased but rather enhanced (Figure 5), which indicates that the $\boldsymbol{S} = 1$ excited energy level is not so high in the presence of methanol, which is evaluated as below 6 K. Although the quantization of modulation depth is difficult, the present result cannot exclude the possibility that the ground and excited states are inverted in the presence of methanol.

Using the point-dipole approximation, the magnetic dipole−dipole interaction from the Mn cluster is described as

$$\epsilon = \gamma_A \mu_B \frac{1 - 3\cos^2\theta}{r^3} \quad (1)$$

where r is the distance between spins A and B, θ is the angle between the distance vector and external magnetic field, and γ_A and μ_B are the gyromagnetic ratio of spin A and the magnetic moment of spin B, respectively. The oscillation of the hole-burning trace is characterized by the fundamental frequency ϵ, and mixing of harmonic frequencies $k\epsilon$ ($k = 2, 3...$) for $\boldsymbol{S} \geq 1$.[29,51] For the cyanobacterial S_1 state, the hole-burning trace was characterized by two fundamental frequencies, 2.56 MHz (period 390 ns) and 1.59 MHz (period 630 ns).

https://doi.org/10.1021/acsphyschemau.5c00068
ACS Phys. Chem Au 2025, 5, 660−671

Assuming a point dipole-approximation for $S = 1$ spin, the distance between $Y_D^\bullet$ and the Mn cluster was evaluated to be 28 Å for the 410 ns period. The distance between $Y_D^\bullet$ and Mn ions in the crystal structure was estimated as 30−33 Å. To compensate for these differences, the Mn ions with positive spin densities should be closer to $Y_D^\bullet$. In the crystal structure, the Mn1 and Mn4 ions are closer to $Y_D^\bullet$ than the Mn2 and Mn3 ions. Therefore, the spin densities of Mn1 and Mn4 are expected to be positive and larger than those of Mn2 and Mn3.

The spin Hamiltonian for manganese cluster is described as

$$\mathcal{H} = -2\sum_{i<j}^{4} J_{ij}\mathbf{S}_i\cdot\mathbf{S}_j \tag{2}$$

$$\mathbf{S}_T = \sum_{i}^{4} \mathbf{S}_i \tag{3}$$

where $\mathbf{S}_T$ is the summation of each spin $\mathbf{S}_i$ on the i-th Mn ion, and J_{ij} is the exchange coupling between the i-th and j-th spins. Considering spin density distribution for $Y_D^\bullet$ and the Mn cluster, the magnetic dipole−dipole interaction can be written as

$$\epsilon = \gamma_A\mu_B \sum_{i,j} \frac{1 - 3\cos^2\theta_{i,j}}{r_{i,j}^3}\rho_i\rho_j \tag{4}$$

where $r_{i,j}$ and $\theta_{i,j}$ are the distance and angle between the external field vector and the vector r_{ij} connecting the spin density ρ_i on the i-th carbon of $Y_D^\bullet$ and ρ_j on the j-th manganese ion, respectively.[24] The spin density distribution of $Y_D^\bullet$ has been previously described,[24] which was fitted from the experimental results. The coordinates were obtained from the crystal structures. The density distribution ρ_j is replaced by the spin projection, which is defined as

$$p_j = \frac{\mathbf{S}_i\cdot\mathbf{S}}{\mathbf{S}^2} \tag{5}$$

$$\sum_{j}^{4} p_j = 1 \tag{6}$$

where p_j represents the contribution of the local spin $\mathbf{S}_i$ to the total spin $\mathbf{S}$. The FID shape is expressed as follows:

$$H_T(t) = H_0(t)f_T(t) \tag{7}$$

where $H_T(t)$ is the entire shape function for the FID, $H_0(t)$ is the function at $T = 0$, and $f_T(t)$ is the shape function for the spectral diffusion.[29,51]

Under the condition of $T \to \infty$ for $S \geq 1$,

$$f_\infty(t) = \frac{1}{2S+1} + \sum_{k=1}^{2s} \frac{2(2S+1-k)}{(2S+1)^2}\cos(k\epsilon t) \tag{8}$$

For $S = 1$ spin,

$$f_\infty(t) = \frac{1}{3}\left[1 + \frac{4}{3}\cos(\epsilon t) + \frac{2}{3}\cos(2\epsilon t)\right] \tag{9}$$

For $S = 3$ spin,

$$f_\infty(t) = \frac{1}{7}\left[1 + \frac{12}{7}\cos(\epsilon t) + \frac{10}{7}\cos(2\epsilon t) + \frac{8}{7}\cos(3\epsilon t) + \frac{6}{7}\cos(4\epsilon t) + \frac{4}{7}\cos(5\epsilon t) + \frac{2}{7}\cos(6\epsilon t)\right] \tag{10}$$

where all transitions in the sublevels are equivalent to t under the condition that $T \gg T_1$. A larger spin enhanced the oscillation depth of the first peak. Because the fundamental frequency ϵ is obviously dominant in the first peak on a trace, these equations were applied to simulate traces as an approximation without considering the T_1 dependence in the sublevel relaxations. In a previous study, $H_0(t)$ was replaced with the minimum experimental conditions for T, $H_{min}(t)$.[51] However, the differences in the traces between $H_{min}(t)$ and $H_T(t)$ were so small that evaluation was difficult. In this study, the experimental results were evaluated by dividing the trace of the S_1 state by that of Mn-depleted PSII, which extracts MDI from manganese cluster. The procedure is used in RIDME.[32] The selective hole-burning traces of Mn-depleted PSII were combined with the effects of nonheme iron, Fe^{2+}, cytochrome (cyt) b_{559}, and cyt c_{550}, etc.

The difference between the point spins (eq 1) and delocalized spin (eq 4) suggests that the spin density distributions on Mn1 and Mn4 are positive and larger than those on Mn2 and Mn3. The distances between $Y_D^\bullet$ and Mn1/Mn4 ions were shorter than those between $Y_D^\bullet$ and Mn2/Mn3. Therefore, the larger positive spin densities for Mn1/Mn4 are expected to be Mn(III). The $S = 1$ spin in the S_1 state is formally explained by a ferro-coupled $S = 1$ spin between two antiferro-coupled $S = 1/2$ Mn(III)−Mn(IV) dimers, that is Mn1−Mn2 and Mn3−Mn4. For an antiferro-coupled Mn(III)−Mn(IV) dimer, the projection was obtained at a ratio of 2:−1.[62] Therefore, the spin density distributions can be formally explained by a simple model in which the spin projection in a single Mn(III)−Mn(IV) dimer was divided by the ratio of 2:−1,[62] and coupled as two dimers. The ratio of the spin density distribution is well conserved in the QM model.[63−65]

Figure 8 shows the experimental and calculated traces of (A) plant PSII in the presence of methanol and (B) *T. vulcanus* PSII. The experimental trace (trace a) was compared with traces b−e, the calculated traces based on the QM models of the S_1 state with $S = 1$. The crystal structure of PDB 6JLJ[66] was used for the calculations. The calculation was performed by summing all polar coordinates (θ, ϕ). Crystal-structure dependence was within 20 ns for the first oscillation peak (Figure S5). For the analysis of the experimental traces, the spin projections were obtained from (b) model S_1A (Drosou et al.(2023)),[63] (c, d) models S_1aR and S_1bR (Isobe et al. (2014)),[64] and (e) model S_1(pre) (Tamura et al. (2023)).[65] The spin projections and J values are listed in Tables 1 and 2, respectively. Figure 9 shows schematic structures for these structures. Although these QM calculations were performed using different methodologies and assumptions, it is worth comparing them from the perspective of structural differences. Main differences of QM calculations are the use of DFT[63,64] or QM/MM,[65] wave function sets, surrounding amino acid residues, and the protonation states of amino acid residues.

The structural differences were mainly due to the protonation state of the oxygen ligands (W1, W2, O4, and O5) in the Mn cluster. The protonation structures for each trace are (b) (W1, W2, O4, O5) = (H_2O, OH^-, O^{2-}, O^{2-}), (c,

https://doi.org/10.1021/acsphyschemau.5c00068
ACS Phys. Chem Au 2025, 5, 660−671

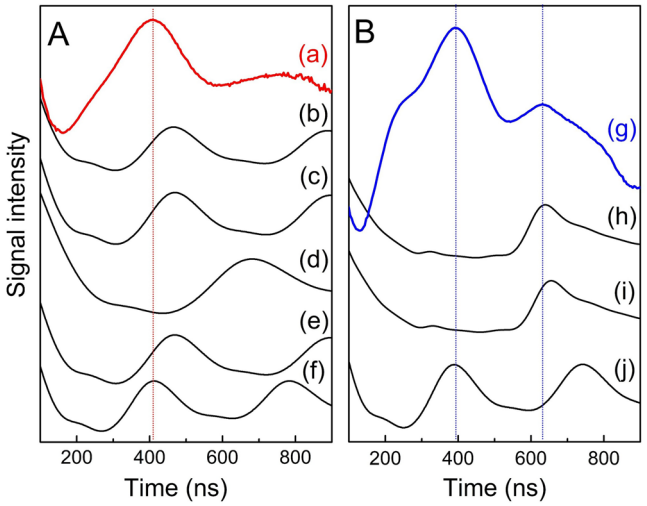

Figure 8. Experimental and calculated traces of selective hole burning of (a) plant PSII in the presence of methanol and (g) untreated *T. vulcanus* PSII. Traces (b, c, d, e, h) are calculated based on (b) model S_1A and (h) model S_1B (Drosou et al.(2023)),[63] (c) model S_1aR, (d) S_1bR (Isobe et al.(2014)),[64] and (e) S_1(pre) (Tamura et al. (2023)).[65] Traces (f, i) are simplified models, using the spin density distribution of (f) [1.6:−1.1:−1.1:1.6] and (j) [1.8:−1.3:−1.3:1.8] for Mn1−4 (S = 1), and (i) [−0.5:0.5:0.5:0.5] for Mn1−4 (S = 3). The dotted lines indicate (A) a period of 410 ns, (B) 390 ns, and 630 ns.

Table 1. Isotropic Spin Density Distributions for Mn1−4[a]

	ρ(Mn1)	ρ(Mn2)	ρ(Mn3)	ρ(Mn4)
S = 1				
(b) S_1A	1.19	−0.66	−0.42	0.89
(c) S_1aR	1.11	−0.60	−0.51	1.00
(d) S_1bR	−0.55	0.39	0.48	0.69
(e) S_1(pre)	1.12	−0.61	−0.49	0.98
(f)	1.60	−1.10	−1.10	1.60
(j)	1.80	−1.30	−1.30	1.80
S = 3				
(h) S_1B	−0.47	0.40	0.49	0.59
(i)	−0.50	0.50	0.50	0.50

[a]Parameters (c, d) were obtained from Isobe et al.[64] Parameters (b, h) and (e) were derived from the J values reported by Drosou et al.[67] and Tamura et al.[65] The parameters for models (c) S_1aR and (d) S_1bR were obtained from the generalized approximate spin projection and adiabatic energy levels.[64]

e) (W1, W2, O4, O5) = (H_2O, H_2O, O^{2-}, O^{2-}), and (d) (W1, W2, O4, O5) = (H_2O, OH^-, O^{2-}, OH^-).

Models (b), (c), and (e) qualitatively reproduced the experimental trace with periods of 460−470 ns. However, model (d) was far from the experimental trace (a), which was estimated to have a period of 690 ns. Generally, a higher-valence ion has a larger spin projection in a coupled spin system. This ratio appears to be inherited in the QM calculations of the four coupled manganese cluster. The isotropic spin densities for the QM models (b, c, e) are approximately [1.0:−0.5:−0.5:1.0] with valence [III, IV, IV, III] for Mn1−4. Trace (f) is a simplified model using the spin ratio [1.6:−1.1:−1.1:1.6] for Mn1−4, which was calculated to adjust the experimental trace using simple two-digit numbers.

In parallel-polarized EPR measurements, two types of S_1 signals were detected: S = 1 in plant PSII and S = 2 or 3 in cyanobacterial PSII.[15−20,50] In comparison with these works, the 400 ns period can be assigned to the S = 1 state, and the 630 ns period can be assigned to S = 2 or 3. In other words, the cyanobacterial S_1 state has an S = 1 spin structure as well as partially the $S \geq 2$ isomer. Figure 8B shows the experimental and calculated traces of untreated *T. vulcanus* PSII. The experimental trace (trace g) was compared with (trace h) calculations based on the S_1 state QM models with S = 3.[63] The protonation state was (h) (W1, W2, O4, O5) = (H_2O, OH^-, O^{2-}, O^{2-}).[63] The spin projections are listed in Table 1. The spin valences and distribution were (h) [III, IV, IV, III] and [−0.47, 0.40, 0.49, 0.59] for Mn1−4, respectively. Trace (i) is a simulated trace using simple two-digit numbers of [−0.5:0.5:0.5:0.5]. This spin distribution was consistent with an earlier report.[50]

It is difficult to quantify the number of states with S = 1 compared with those with $S \geq 2$. However, the oscillation depth of the higher spin state is greater than that of the low spin state; therefore, the amount of $S \geq 2$ can be much smaller than that of S = 1.

We obtained a 400 ns period for S = 1 and a 630 ns period for $S \geq 2$. The results showed that the cyanobacterial S_1 state is composed of two isomers. For cyanobacterial PSII, the parallel-polarized S_1 signal was assigned to the S = 2 or S = 3 ground states.[50] The selective hole-burning experiments cannot specify the absolute spin number of the $S \geq 2$ spin state because the main period of the selective hole-burning trace is characterized by the fundamental frequency ϵ and is not very sensitive to the spin number (Figure S6). As the QM calculation indicates that the $S \geq 2$ spin state arises from S = 3,[67] we tentatively assigned that the observed periods arise from S = 1 and S = 3.

The MDI for the $Y_D^{\bullet}$-S_2 state is similar to that for the $Y_D^{\bullet}$-S_1 state, but the interactions of the $Y_D^{\bullet}$-S_0 state are largely different from those of the $Y_D^{\bullet}$-S_1 state. The MDI are 1.2 MHz

Table 2. *J*-Coupling Sets and Structure for the S_1 State in the Reported QM Structures (cm^{-1})[a]

	J_{12}	J_{13}	J_{14}	J_{23}	J_{24}	J_{34}	ΔE	W1	W2	O4	O5
S = 1											
(b) model S_1A	−22.0	8.5	3.83	19.6	0.25	−72.1	26.2	H_2O	OH^-	O^{2-}	O^{2-}
(c) model 1aR	−35.6	6.84	0.11	18.4	2.91	−77.1	1.86	H_2O	H_2O	O^{2-}	O^{2-}
(d) model 1bR	−36.5	−2.04	−4.04	4.27	0.44	−8.14	14.0	H_2O	OH^-	O^{2-}	OH^-
(e) model S_1 (pre)	−36.2	7.4	0.6	13.8	0.70	−78.1	0.49	H_2O	H_2O	O^{2-}	O^{2-}
S = 3											
(h) model S_1B	−35.9	3.85	−15.8	30.2	−0.52	5.38	78.9	H_2O	OH^-	O^{2-}	O^{2-}

[a]Parameters for (b) model S_1A and (e) model S_1(pre) were taken from refs 67 and 65, respectively. The parameters for models (c) S_1aR and (d) S_1bR were obtained from the generalized approximate spin projection, adiabatic energy levels.[64] ΔE is the energy gap between the ground and excited states. The states are located at the (b−d) first excited states and the (e, h) ground state.

https://doi.org/10.1021/acsphyschemau.5c00068
ACS Phys. Chem Au 2025, 5, 660−671

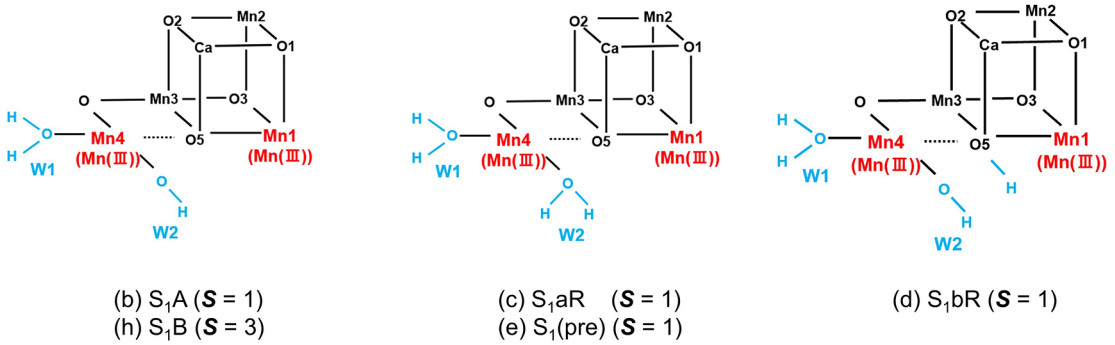

Figure 9. Schematic models of QM calculations. The models were obtained from (b) model S_1A (Drosou et al.(2023)),[63] (c, d) models S_1aR and S_1bR (Isobe et al.(2014)),[64] and (e) model S_1(pre) (Tamura et al. (2023)).[65]

(850 ns) and 2.4 MHz (420 ns) MHz for the S_0[26] and S_2 states,[24] respectively. The small MDI for the S_0 state excludes the possibility that the minor population of the S_0 state influences the observation of the S_1 state.

At present, the origin of the 256 ns period is unclear. As observed in the PsbP/Q- and PsbO/P/Q-depleted spinach PSII, the period did not correlate with the $S = 1$ and $S = 3$ spin. The period was estimated to be 22 Å using the point dipole approximation, which is so close that it could not be assigned to the Mn cluster, and there are no other candidates for the spin center.

Different QM models have been reported, particularly for the protonation states. The protonation state of (W1, W2, O4, O5) = (H_2O, OH^-, O^{2-}, OH^-) (S_1bR) (trace d) was excluded from the S_1 state model. Some spin density distributions in the QM calculations (traces b, c and e) were similar, even under different protonation conditions. These states are distinguishable using the results of parallel polarization EPR.[15−20,50] The first excitation energy for model S_1A (W1, W2, O4, O5) = (H_2O, OH^-, O^{2-}, O^{2-}) was calculated as 26.2 cm^{-1} (37.8 K) (Table 2). This was so high that model S_1A did not fit the parallel-polarization EPR experiments. The excited energy for the model (W1, W2, O4, O5) = (H_2O, H_2O, O^{2-}, O^{2-}) is 1.86 cm^{-1} (2.67 K) for S_1aR (trace c)[64] and 0.49 cm^{-1} (0.70 K) for S_1(pre) (trace e),[65] respectively. The differences between (c) and (e) can be ascribed to the different methodologies used, that is, (c) DFT[64] and (e) QM/MM.[65] Although it depends on the choice of the basis function, the energy gap between the two models is relatively smaller than that in the other models, estimated as below 9 cm^{-1}.[64] These results suggest that the model of (W1, W2, O4, O5) = (H_2O, H_2O, O^{2-}, O^{2-}) is preferable to explain the parallel-polarization EPR experiments,[19] which show a weakly excited state of 1.7 cm^{-1} (2.5 K) for the S_1 state.

The zero-field splitting parameters provided additional information for the $S = 1$ state. The disappearance of the parallel-polarized signal with methanol was ascribed to the symmetrized crystalline field, that is, a decrease in the E/D ratio. Drosou et al. calculated the effective $|D|$ in the range of 0.15 −1.0 cm^{-1}, and the corresponding $|E/D|$ in the range of 0.16−0.33, for $S = 1$ state.[67] However, Matsukawa et al. have already estimated $|D| = 0.14$ cm^{-1} and $|E/D| = 0.11$, and the effective $\boldsymbol{D}$ is along the membrane plane in the oriented PSII.[20]

The effective $\boldsymbol{D}$ is represented as the sum of the local zero-field splitting of each Mn ion and the interactions between the Mn ions:

$$\boldsymbol{D} = \sum_{i=1}^{4} \boldsymbol{d}_{\mathrm{loc},i} + \sum_{i>j}^{4} \boldsymbol{d}_{ij} \tag{11}$$

where $\boldsymbol{d}_{\mathrm{loc},j}$ is the local zero-field splitting for the i-th Mn ion, and $\boldsymbol{d}_{ij}$ is the interaction between the i-th and j-th Mn ions. Assuming that the local zero-field splitting of Mn(III), $\boldsymbol{d}_{\mathrm{Mn(III)}}$, is much larger than that of Mn(IV), $\boldsymbol{d}_{\mathrm{Mn(IV)}}$,[68] the effective $\boldsymbol{D}$ was evaluated as the sum of the local $\boldsymbol{d}_{\mathrm{Mn(III)}}$ of Mn1 and Mn4. In the QM model (W1, W2, O4, O5) = (H_2O, OH^-, O^{2-}, O^{2-}), the Jahn−Teller axes were assumed to be directed toward Asp170-Mn4-Glu333 for Mn4 and Asp342-Mn1-O5 for Mn1. These axes were located outside the membrane plane (Figure S7). This study showed that the spin projections of Mn1 and Mn4 were both positive, indicating that the local spins of Mn1 and Mn4 were oriented toward the total spin S_z. Assuming that the local $\boldsymbol{d}_{\mathrm{Mn(III)}}$ values for Mn1 and Mn4 have the same sign and comparable magnitude, the resultant vector will be along the membrane plane (Figure S7), which is consistent with the experimental results.[69] Britt et al. evaluated the sign of the effective D for the S_1 state signal ($S = 2$) as positive based on temperature dependence.[50] The zero-field parameter $\boldsymbol{d}_{\mathrm{Mn(III)}}$ is generally negative in coordinates elongated by the Jahn−Teller effect.[68] Only Mn1 had a negative spin density of −0.5. Assuming that the local zero-field splitting of Mn1 is dominant for the effective $\boldsymbol{D}$ in the $\boldsymbol{S} \geq 2$ state, the sign of the effective D becomes positive, which is consistent with the experimental results.[50] On the other hand, Mn(IV) ions with high $\boldsymbol{d}_{\mathrm{Mn(IV)}}$ have also been reported.[70] The local zero-field splitting of Mn2 and Mn3 and the interactions between the Mn ions should be considered for a precise discussion.

The $\boldsymbol{S} = 1$ QM models (traces b, c, e) were characterized by an isotropic spin distribution [1.0:−0.5:−0.5:1.0]; however, the experimental trace fits the ratio [1.6:−1.1:−1.1:1.6] or [1.8:−1.3:−1.3:1.8]. The $\boldsymbol{S} = 3$ model for the QM calculation was qualitatively reproduced by the experimental results, which were characterized by a simple isotropic spin distribution [−0.5:0.5:0.5:0.5]. The differences between the $\boldsymbol{S} = 1$ and $\boldsymbol{S} = 3$ states indicate that the boundary conditions for $\boldsymbol{S} = 1$ may be insufficient for reproducing the structures. The equilibrium between the two isomers, $\boldsymbol{S} = 1$ and $\boldsymbol{S} = 3$, is induced by the extrinsic proteins PsbP/Q in spinach PSII.[17] Similar isomerization was detected in the S_2 state between the $g = 2$ multiline and $g = 4$ signals.[47] As the arrangement of amino acid residues around the Mn cluster was almost the same in plant and cyanobacterial PSII, this isomerization was thought to be due to a remote effect, probably a chain of hydrogen bonds.[47]

https://doi.org/10.1021/acsphyschemau.5c00068
ACS Phys. Chem Au 2025, 5, 660−671

Generally, the valence of the Mn ions is believed to be 2Mn(III)2Mn(IV) in the S_1 state, which is called a high-valence model. Low-valence models such as 4Mn(III) have also been proposed.[71−74] Based on these reports, Pantazis evaluated the spin structures of the low-valence models.[75] Two different types of spin states were proposed: model 1 with valence [III, III, III, III] for Mn1−4, and model 2 with valence [III, IV, III, II]. Model 1 has a ground state S = 4 and four excited states S = 0, 1, 2, 3 below 3.1 cm^{-1}. Such multiple-overlapping excited states do not fit with the present work or previous EPR results[50] for the S_1 state. Model 2 has ground states of S = 0 and S = 1, with a high excited state of 25.5 cm^{-1}. The isotropic spin density distribution was [0.49:0.01:−0.03:0.54] for Mn1−4, which was calculated from the J-set.[75] These states also do not fit with the present work or previous EPR results.[19] To the best of our knowledge, no other spin analyses of QM calculations have been reported for the low-valence models. Currently, we do not support low-valence models for the S_1 state. The possibility that other low-valence models explain the EPR results cannot be excluded; however, further research is required.

The extrinsic proteins PsbO/P/Q for plant PSII and PsbO/U/V for cyanobacterial PSII protect the Mn cluster. PsbP is directly related to the function of the manganese cluster.[54,76] A Fourier transform infrared spectroscopy study showed that PsbP is coupled to the structure of the oxygen-evolving complex, and the binding of the PsbP protein influences the protein conformation around the Mn cluste.[54] During the transition of the S_1-to-S_2 state, PsbP depletion modified the local environment but did not modify the manganese ligands. Parallel-polarization EPR showed that PsbP/Q depletion was caused by modification of the microenvironment, which produced the $S \geq 2$ isomer.[17,50] However, in the selective hole-burning measurements, the 630 ns period ($S \geq 2$) was not detected with the decrease of the 410 ns period (S = 1) in either PsbP/Q-depleted or PsbO/P/Q-depleted PSII. This indicated that PsbP depletion modified the surrounding environment of the Mn cluster, resulting in a distance distribution of Mn and $Y_D^{\bullet}$. In the canonical distribution, PSII centers might partly have the $S \geq 2$ isomer. The oscillations in PsbO/U/V-depleted *T. vulcanus* PSII were almost the same as those in untreated *T. vulcanus* PSII in the presence of PEG (Figure 7). In the absence of PEG, the $S \geq 2$ isomer was not detected with a slight modification of S = 1, indicating that PEG is also fixing the Mn-cluster in the absence of extrinsic proteins. These results show that PsbO/U/V fix the S_1 state Mn cluster in cyanobacterial PSII similar to PsbO/P/Q in higher plant PSII, but the effects of these sets of extrinsic proteins are different.

In the S_2 state, PsbO supports the isomerization of the Mn cluster. Plant PSII has an S = 5/2 isomer in the S_2 state but is lost by the depletion of PsbO. In contrast, the cyanobacterial PSII does not contain the S = 5/2 isomer. Therefore, the $S \geq 2$ isomer in the S_1 state cannot be the precursor to the isomer S = 5/2 in the S_2 state. As the amount of the $S \geq 2$ isomer in the S_1 state is relatively small, the main path for S_1-to-S_2 states transition would be S = 1 to S = 1/2 structures.

To elucidate the reaction mechanism of Mn cluster, it is essential to understand the effects of the microenvironment created by extrinsic proteins. Although such remote effects may be difficult to introduce into the present QM calculations, it would be worthwhile to include them in the computational procedure.

In this study, two protonation states in the QM calculations matched the selective hole-burning experiments: (W1, W2, O4, O5) = (H_2O, H_2O, O^{2-}, O^{2-}) for the S = 1 spin state, and (W1, W2, O4, O5) = (H_2O, OH^-, O^{2-}, O^{2-}) for the S = 3 spin state. However, the following points should be considered: (1) For the S = 1 state, the QM models give rise to an isotropic spin distribution of approximately [1.0:−0.5:−0.5:1.0] for Mn1−4, which does not completely reproduce the experimental trace. Additional boundary conditions were considered. (2) Drosou et al. have reported the S = 3 model.[67] The QM model focused on the protonation conditions of W2 = OH^-, which were inherited from the original S_2 model.[22] When S = 1, the protonation of W2 was not very sensitive to the spin density distribution (Figure 8). For the S = 3 state, the stability of the spin states should also be discussed along with other possible structures. As S = 3 structure is inherited from the S = 1 structure as isomer, the S_1 state should also have the (W1, W2, O4, O5) = (H_2O, H_2O, O^{2-}, O^{2-}) structure.

CONCLUSIONS

The magnetic dipole−dipole interactions between $Y_D^{\bullet}$ and the S_1 state Mn cluster in PSII were detected using selective hole-burning Q-band pulsed EPR for both spinach and cyanobacterial PSII. The interactions were characterized by two fundamental periods at 410 (390) ns and 630 ns. The former was detected in both the plant and cyanobacterial PSII, ascribed to S = 1 spin, and the latter was detected only in the cyanobacterial PSII, ascribed to $S \geq 2$ spin. The basic structure of the S_1 state is S = 1, and the $S \geq 2$ isomer is included in the cyanobacterial PSII. Some QM models with S = 1 and S = 3 were consistent with the experimental results, depending on the protonation conditions of the Mn cluster. In the simplified models, the isotropic spin density distributions are explained as the ratio [1.6:−1.1:−1.1:1.6] or [1.8:−1.3:−1.3:1.8] for Mn1−4 ions at S = 1 and [−0.5:0.5:0.5:0.5] for Mn1−4 ions at S = 3. The most probable protonated structures were W1 = H_2O, W2 = H_2O, O4 = O^{2-}, and O5 = O^{2-} for the S_1 state. Because the S_1 state is the most reliable structure for X-ray analysis, this study will be useful for refining electronic structures.

These results demonstrate that the selective hole burning method is a powerful complementary tool to XRD for determining the valence and protonation structures of manganese clusters. This technique is valid not only for the S_1 state but also for higher S-states and general metal clusters. This provides important insights into the water oxidation mechanism.

ASSOCIATED CONTENT

Supporting Information

The Supporting Information is available free of charge at https://pubs.acs.org/doi/10.1021/acsphyschemau.5c00068.

Figure S1. Selective hole-burning traces of spinach S_1 state PSII in the presence of 3% MeOH; **Figure S2.** Selective hole-burning traces of *T. vulcanus* S_1 state PSII; **Figure S3.** Selective hole-burning traces of Mn-depleted spinach PSII; **Figure S4.** Selective hole-burning traces of Mn-depleted *T. vulcanus* PSII; **Figure S5.** Selective hole-burning traces calculated in different crystal structures; **Figure S6.** Selective hole-burning traces calculated using different spin numbers; **Figure S7.** Orientation of the local D_Z for Mn1 and Mn4 in the crystal structure (PDF)

https://doi.org/10.1021/acsphyschemau.5c00068
ACS Phys. Chem Au 2025, 5, 660−671

AUTHOR INFORMATION

Corresponding Author

Hiroyuki Mino − *Department of Physics, Graduate School of Science, Nagoya University, Nagoya 464-8602 Aichi, Japan;* orcid.org/0000-0003-4040-8732; Email: mino@bio.phys.nagoya-u.ac.jp

Authors

Shinya Kosaki − *Department of Physics, Graduate School of Science, Nagoya University, Nagoya 464-8602 Aichi, Japan*

Naohiko Nakamura − *Department of Physics, Graduate School of Science, Nagoya University, Nagoya 464-8602 Aichi, Japan*

Yoshiki Nakajima − *Research Institute for Interdisciplinary Science, Advanced Research Field, and Graduate School of Environmental, Life, Natural Science and Technology, Okayama University, Okayama 700-8530, Japan;* orcid.org/0000-0002-0529-8075

Jian-Ren Shen − *Research Institute for Interdisciplinary Science, Advanced Research Field, and Graduate School of Environmental, Life, Natural Science and Technology, Okayama University, Okayama 700-8530, Japan;* orcid.org/0000-0003-4471-8797

Complete contact information is available at: https://pubs.acs.org/10.1021/acsphyschemau.5c00068

Notes

The authors declare no competing financial interest.

ACKNOWLEDGMENTS

This work was partly supported by the Advanced Research Infrastructure for Materials and Nanotechnology in Japan (ARIM) of MEXT, Institute for Molecular Science (JPMXP1224MS1016/JPMXP1225MS1014 to H.M.), JSPS KAKENHI (Grant Number 22K06160/24H02078 to H.M.), and JSPS KAKENHI (Grant Number JP22H04916 to J.-R.S.), and supported by MEXT Promotion of Development of a Joint Usage/Research System Project: Coalition of Universities for Research Excellence Program (CURE) Grant Number JPMXP1323015488 (Spin-L program No, spin23XN007 and spin25XN018).

ABBREVIATIONS

QM, quantum mechanical; QM/MM, quantum mechanics/molecular mechanics; EPR, electron paramagnetic resonance; ENDOR, electron nuclear double resonance; ESEEM, electron spin−echo envelope modulation; XFEL, X-ray free electron laser; EXAFS, extended X-ray absorption fine structure; MES, 2-(N-morpholino) ethanesulfonic acid; ESE, electron spin echo; mw, microwave; FID, free induction decay; MDI, magnetic dipole interaction; RIDME, Relaxation-induced dipolar modulation enhancement; PELDOR, Pulsed electron−electron double resonance; MDI, magnetic dipole interaction.

REFERENCES

(1) Shen, J. R. The Structure of Photosystem II and the Mechanism of Water Oxidation in Photosynthesis. *Annu. Rev. Plant Biol.* **2015**, *66*, 23−48.

(2) Yano, J.; Yachandra, V. Mn_4Ca Cluster in Photosynthesis: Where and How Water is Oxidized to Dioxygen. *Chem. Rev.* **2014**, *114*, 4175−4205.

(3) Lubitz, W.; Pantazis, D. A.; Cox, N. Water oxidation in oxygenic photosynthesis studied by magnetic resonance techniques. *FEBS Lett.* **2023**, *597*, 6.

(4) Umena, Y.; Kawakami, K.; Shen, J. R.; Kamiya, N. Crystal structure of oxygen-evolving photosystem II at a resolution of 1.9 Å. *Nature* **2011**, *473*, 55−60.

(5) Li, H. J.; Nakajima, Y.; Nango, E.; Owada, S.; Yamada, D.; Hashimoto, K.; Luo, F. J.; Tanaka, R.; Akita, F.; Kato, K.; Kang, J. M.; Saitoh, Y.; Kishi, S.; Yu, H. X.; Matsubara, N.; Fujii, H.; Sugahara, M.; Suzuki, M.; Masuda, T.; Kimura, T.; Thao, T. N.; Yonekura, S.; Yu, L. J.; Tosha, T.; Tono, K.; Joti, Y.; Hatsui, T.; Yabashi, M.; Kubo, M.; Iwata, S.; Isobe, H.; Yamaguchi, K.; Suga, M.; Shen, J. R. Oxygen-evolving photosystem II structures during S_1-S_2-S_3 transitions. *Nature* **2024**, *626*, 670−677.

(6) Suga, M.; Akita, F.; Yamashita, K.; Nakajima, Y.; Ueno, G.; Li, H. J.; Yamane, T.; Hirata, K.; Umena, Y.; Yonekura, S.; Yu, L. J.; Murakami, H.; Nomura, T.; Kimura, T.; Kubo, M.; Baba, S.; Kumasaka, T.; Tono, K.; Yabashi, M.; Isobe, H.; Yamaguchi, K.; Yamamoto, M.; Ago, H.; Shen, J. R. An oxyl/oxo mechanism for oxygen-oxygen coupling in PSII revealed by an x-ray free-electron laser. *Science* **2019**, *366*, 334−338.

(7) Kern, J.; Chatterjee, R.; Young, I. D.; Fuller, F. D.; Lassalle, L.; Ibrahim, M.; Gul, S.; Fransson, T.; Brewster, A. S.; Alonso-Mori, R.; Hussein, R.; Zhang, M.; Douthit, L.; de Lichtenberg, C.; Cheah, M. H.; Shevela, D.; Wersig, J.; Seuffert, I.; Sokaras, D.; Pastor, E.; Weninger, C.; Kroll, T.; Sierra, R. G.; Aller, P.; Butryn, A.; Orville, A. M.; Liang, M. N.; Batyuk, A.; Koglin, J. E.; Carbajo, S.; Boutet, S.; Moriarty, N. W.; Holton, J. M.; Dobbek, H.; Adams, P. D.; Bergmann, U.; Sauter, N. K.; Zouni, A.; Messinger, J.; Yano, J.; Yachandra, V. K. Structures of the intermediates of Kok's photosynthetic water oxidation clock. *Nature* **2018**, *563*, 421−425.

(8) Bhowmick, A.; Hussein, R.; Bogacz, I.; Simon, P. S.; Ibrahim, M.; Chatterjee, R.; Doyle, M. D.; Cheah, M. H.; Fransson, T.; Chernev, P.; Kim, I. S.; Makita, H.; Dasgupta, M.; Kaminsky, C. J.; Zhang, M.; Gaetcke, J.; Haupt, S.; Nangca, I. I.; Keable, S. M.; Aydin, A. O.; Tono, K.; Owada, S.; Gee, L. B.; Fuller, F. D.; Batyuk, A.; Alonso-Mori, R.; Holton, J. M.; Paley, D. W.; Moriarty, N. W.; Mamedov, F.; Adams, P. D.; Brewster, A. S.; Dobbek, H.; Sauter, N. K.; Bergmann, U.; Zouni, A.; Messinger, J.; Kern, J.; Yano, J.; Yachandra, V. K. Structural evidence for intermediates during O_2 formation in photosystem II. *Nature* **2023**, *617*, 629−636.

(9) Suga, M.; Akita, F.; Sugahara, M.; Kubo, M.; Nakajima, Y.; Nakane, T.; Yamashita, K.; Umena, Y.; Nakabayashi, M.; Yamane, T.; Nakano, T.; Suzuki, M.; Masuda, T.; Inoue, S.; Kimura, T.; Nomura, T.; Yonekura, S.; Yu, L. J.; Sakamoto, T.; Motomura, T.; Chen, J. H.; Kato, Y.; Noguchi, T.; Tono, K.; Joti, Y.; Kameshima, T.; Hatsui, T.; Nango, E.; Tanaka, R.; Naitow, H.; Matsuura, Y.; Yamashita, A.; Yamamoto, M.; Nureki, O.; Yabashi, M.; Ishikawa, T.; Iwata, S.; Shen, J. R. Light-induced structural changes and the site of O = O bond formation in PSII caught by XFEL. *Nature* **2017**, *543*, 131−135.

(10) Amin, M. Predicting the oxidation states of Mn ions in the oxygen-evolving complex of photosystem II using supervised and unsupervised machine learning. *Photosyn. Res.* **2023**, *156*, 89−100.

(11) Yamaguchi, K.; Miyagawa, K.; Shoji, M.; Kawakami, T.; Isobe, H.; Yamanaka, S.; Nakajima, T. Theoretical elucidation of the structure, bonding, and reactivity of the $CaMn_4O_x$ clusters in the whole Kok cycle for water oxidation embedded in the oxygen evolving center of photosystem II. New molecular and quantum insights into the mechanism of the O-O bond formation. *Photosyn. Res.* **2024**, *162*, 291−330.

(12) Siegbahn, P. E. M. A quantum chemical approach for the mechanisms of redox-active metalloenzymes. *RSC Adv.* **2021**, *11*, 3495−3508.

(13) Ishikita, H.; Saito, K. Photosystem II: Probing Protons and Breaking Barriers. *Biochemistry* **2025**, *64*, 1895−1906.

(14) Styring, S.; Rutherford, A. W. In the oxygen-evolving complex of photosystem II the S_0 state is oxidized to the S_1 state by D^+ (signal-II_{slow}). *Biochemistry* **1987**, *26*, 2401−2405.

(15) Dexheimer, S. L.; Klein, M. P. Detection of a Paramagnetic Intermediate in the S_1-state of the Photosynthetic Oxygen-Evolving Complex. *J. Am. Chem. Soc.* **1992**, *114*, 2821−2826.
(16) Campbell, K. A.; Force, D. A.; Nixon, P. J.; Dole, F.; Diner, B. A.; Britt, R. D. Dual-mode EPR detects the initial intermediate in photoassembly of the photosystem II mn cluster: The influence of amino acid residue 170 of the D1 polypeptide on Mn coordination. *J. Am. Chem. Soc.* **2000**, *122*, 3754−3761.
(17) Campbell, K. A.; Gregor, W.; Pham, D. P.; Peloquin, J. M.; Debus, R. J.; Britt, R. D. The 23 and 17 kDa extrinsic proteins of photosystem II modulate the magnetic properties of the S_1-state manganese cluster. *Biochemistry* **1998**, *37*, 5039−5045.
(18) Campbell, K. A.; Peloquin, J. M.; Pham, D. P.; Debus, R. J.; Britt, R. D. Parallel polarization EPR detection of an S_1-state "multiline" EPR signal in photosystem II particles from Synechocystis sp. PCC 6803. *J. Am. Chem. Soc.* **1998**, *120*, 447−448.
(19) Yamauchi, T.; Mino, H.; Matsukawa, T.; Kawamori, A.; Ono, T. Parallel polarization electron paramagnetic resonance studies of the S_1 state manganese cluster in the photosynthetic oxygen-evolving system. *Biochemistry* **1997**, *36*, 7520−7526.
(20) Matsukawa, T.; Kawamori, A.; Mino, H. Electron paramagnetic resonance study of the magnetic structure of the S_1-state in oriented oxygen evolving photosystem II membranes. *Spectrochim. Acta, Part A* **1999**, *55*, 895−901.
(21) Dismukes, G. C.; Siderer, Y. Intermediates of a Polynuclear Manganese Center Involved in Photosynthetic Oxidation of Water. *Proc. Natl. Acad. Sci. U.S.A.* **1981**, *78*, 274−278.
(22) Ames, W.; Pantazis, D. A.; Krewald, V.; Cox, N.; Messinger, J.; Lubitz, W.; Neese, F. Theoretical evaluation of structural models of the S_2 state in the oxygen evolving complex of Photosystem II: protonation states and magnetic interactions. *J. Am. Chem. Soc.* **2011**, *133*, 19743−19757.
(23) Hara, H.; Kawamori, A.; Astashkin, A. V.; Ono, T. The distances from tyrosine D to redox-active components on the donor side of Photosystem II determined by pulsed electron-electron double resonance. *Biochim. Biophys. Acta* **1996**, *1276*, 140−146.
(24) Asada, M.; Nagashima, H.; Koua, F. H. M.; Shen, J. R.; Kawamori, A.; Mino, H. Electronic structure of S_2 state of the oxygen-evolving complex of photosystem II studied by PELDOR. *Biochim. Biophys. Acta* **2013**, *1827*, 438−445.
(25) Saito, K.; Nishio, S.; Asada, M.; Mino, H.; Ishikita, H. Insights into the protonation state and spin structure for the g = 2 multiline EPR signal of the oxygen-evolving complex. *PNAS Nexus* **2023**, *2*, No. pgad244.
(26) Bittl, R.; Kawamori, A. Configuration of Electron Transfer Components Studied by EPR Spectroscopy, in Photosystem II. In *Photosystem II*; Springer, 2005.
(27) Milov, A. D.; Salikhov, K. M.; Shirov, M. D. Application of ELDOR in Electron-Spin Echo for Paramagnetic Center Space Distribution in Solids. *Fiz. Tverd. Tela.* **1981**, *23*, 975−982.
(28) Dzuba, S. A.; Kawamori, A. Selective hole burning in EPR: Spectral diffusion and dipolar broadening. *Concepts Magn. Reson.* **1996**, *8*, 49−61.
(29) Dzuba, S. A.; Kodera, Y.; Hara, H.; Kawamori, A. The Use of Selective Hole-Burning in EPR-Spectra to Study Spectral Diffusion and Dipolar Broadening. *J. Magn. Reson. A* **1993**, *102*, 257−260.
(30) Wacker, T.; Sierra, G. A.; Schweiger, A. The Concept of FID-Detected Hole-Burning in Pulsed EPR Spectroscopy. *Isr. J. Chem.* **1992**, *32*, 305−322.
(31) Kulik, L. V.; Dzuba, S. A.; Grigoryev, I. A.; Tsvetkov, Y. D. Electron dipole-dipole interaction in ESEEM of nitroxide biradicals. *Chem. Phys. Lett.* **2001**, *343*, 315−324.
(32) Astashkin, A. V. Mapping the Structure of Metalloproteins with RIDME. *Electron Paramagnetic Resonance Investigations of Biological Systems by Using Spin Labels, Spin Probes, and Intrinsic Metal Ions, Pt A* **2015**, *563*, 251−284.
(33) Casey, J. L.; Sauer, K. Electron-Paramagnetic-Res Detection of a Cryogenically Photogenerated Intermediate in Photosynthetic Oxygen Evolution. *Biochim. Biophys. Acta* **1984**, *767*, 21−28.
(34) Zimmermann, J. L.; Rutherford, A. W. EPR Studies of The Oxygen-Evolving Enzyme of Photosystem-II. *Biochim. Biophys. Acta* **1984**, *767*, 160−167.
(35) de Paula, J. C.; Beck, W. F.; Miller, A. F.; Wilson, R. B.; Brudvig, G. W. Studies of the Manganese Site of Photosystem II by Electron Spin Resonance Spectroscopy. *J. Chem. Soc., Faraday Trans. 1* **1987**, *83*, 3635−3651.
(36) Zimmermann, J. L.; Rutherford, A. W. Electron-Paramagnetic Resonance Properties of The S_2 State of the Oxygen-Evolving Complex of Photosystem II. *Biochemistry* **1986**, *25*, 4609−4615.
(37) Messinger, J.; Nugent, J. H. A.; Evans, M. C. W. Detection of an EPR multiline signal for the S_0 state in photosystem II. *Biochemistry* **1997**, *36*, 11055−11060.
(38) Nagashima, H.; Mino, H. Location of Methanol on the S_2 State Mn Cluster in Photosystem II Studied by Proton Matrix Electron Nuclear Double Resonance. *J. Phys. Chem. Lett.* **2017**, *8*, 621−625.
(39) Oyala, P. H.; Stich, T. A.; Stull, J. A.; Yu, F.; Pecoraro, V. L.; Britt, R. D. Pulse electron paramagnetic resonance studies of the interaction of methanol with the S_2 state of the Mn_4O_5Ca cluster of photosystem II. *Biochemistry* **2014**, *53*, 7914−7928.
(40) Chrysina, M.; Heyno, E.; Kutin, Y.; Reus, M.; Nilsson, H.; Nowaczyk, M. M.; DeBeer, S.; Neese, F.; Messinger, J.; Lubitz, W.; Cox, N. Five-coordinate Mn(IV) intermediate in the activation of nature's water splitting cofactor. *Proc. Natl. Acad. Sci. U.S.A.* **2019**, *116*, 16841−16846.
(41) Retegan, M.; Krewald, V.; Mamedov, F.; Neese, F.; Lubitz, W.; Cox, N.; Pantazis, D. A. A five-coordinate Mn(IV) intermediate in biological water oxidation: spectroscopic signature and a pivot mechanism for water binding. *Chem. Sci.* **2016**, *7*, 72−84.
(42) Pantazis, D. A.; Ames, W.; Cox, N.; Lubitz, W.; Neese, F. Two interconvertible structures that explain the spectroscopic properties of the oxygen-evolving complex of photosystem II in the S_2 state. *Angew. Chem., Int. Ed. Engl.* **2012**, *51*, 9935−9940.
(43) Isobe, H.; Shoji, M.; Yamanaka, S.; Umena, Y.; Kawakami, K.; Kamiya, N.; Shen, J. R.; Yamaguchi, K. Theoretical Illumination of Water-inserted Structures of the $CaMn_4O_5$ cluster in the S_2 and S_3 States of Oxygen-Evolving Complex of photosystem II: Full Geometry Optimizations by B3LYP Hybrid Density Functional. *Dalton Trans.* **2012**, *41*, 13727−13740.
(44) Kosaki, S.; Mino, H. Molecular Structure Related to an S = 5/2 High-Spin S_2 State Manganese Cluster of Photosystem II Investigated by Q-Band Pulse EPR Spectroscopy. *J. Phys. Chem. B* **2023**, *127*, 6441−6448.
(45) Cullen, M.; Ray, N.; Husain, S.; Nugent, J.; Nield, J.; Purton, S. A highly active histidine-tagged *Chlamydomonas reinhardtii* Photosystem II preparation for structural and biophysical analysis. *Photochem. Photobiol. Sci.* **2007**, *6*, 1177−1183.
(46) Taguchi, S.; Noguchi, T.; Mino, H. Molecular Structure of the S_2 State with a g = 5 Signal in the Oxygen Evolving Complex of Photosystem II. *J. Phys. Chem. B* **2020**, *124*, 5531−5537.
(47) Taguchi, S.; Shen, L. L.; Han, G. Y.; Umena, Y.; Shen, J. R.; Noguchi, T.; Mino, H. Formation of the High-Spin S_2 State Related to the Extrinsic Proteins in the Oxygen Evolving Complex of Photosystem II. *J. Phys. Chem. Lett.* **2020**, *11*, 8908−8913.
(48) Boussac, A.; Rutherford, A. W.; Sugiura, M. Electron transfer pathways from the S_2-states to the S_3-states either after a Ca^{2+}/Sr^{2+} or a Cl^-/I^- exchange in Photosystem II from *Thermosynechococcus elongatus*. *Biochim. Biophys. Acta* **2015**, *1847*, 576−586.
(49) Boussac, A.; Ugur, I.; Marion, A.; Sugiura, M.; Kaila, V. R. I.; Rutherford, A. W. The low spin - high spin equilibrium in the S_2-state of the water oxidizing enzyme. *Biochim. Biophys. Acta* **2018**, *1859*, 342−356.
(50) Britt, R. D.; Peloquin, J. M.; Campbell, K. A. Pulsed and parallel-polarization EPR characterization of the photosystem II oxygen-evolving complex. *Annu. Rev. Biophys. Biomol. Struct.* **2000**, *29*, 463−495.
(51) Kodera, Y.; Dzuba, S. A.; Hara, H.; Kawamori, A. Distances from tyrosine D^+ to the manganese cluster and the acceptor iron in

https://doi.org/10.1021/acsphyschemau.5c00068
ACS Phys. Chem Au 2025, 5, 660−671

photosustem II as determined by selective hole-burning in EPR spectra. *Biochim. Biophys. Acta* **1994**, *1186*, 91−99.
(52) Mino, H. Temperature dependence of the formation of the g ∼ 5 EPR signal in the oxygen evolving complex of photosystem II. *Photosyn. Res.* **2022**, *152*, 207−212.
(53) Shen, J. R.; Kamiya, N. Crystallization and the crystal properties of the oxygen-evolving photosystem II from Synechococcus vulcanus. *Biochemistry* **2000**, *39*, 14739−14744.
(54) Tomita, M.; Ifuku, K.; Sato, F.; Noguchi, T. FTIR Evidence That the PsbP Extrinsic Protein Induces Protein Conformational Changes around the Oxygen-Evolving Mn Cluster in Photosystem II. *Biochemistry* **2009**, *48*, 6318−6325.
(55) Nagao, R.; Tomo, T.; Noguchi, T. Effects of Extrinsic Proteins on the Protein Conformation of the Oxygen-Evolving Center in Cyanobacterial Photosystem II As Revealed by Fourier Transform Infrared Spectroscopy. *Biochemistry* **2015**, *54*, 2022−2031.
(56) Hallahan, B. J.; Nugent, J. H. A.; Warden, J. T.; Evans, M. C. W. Investigation of the origin of the S_3 EPR signal from the oxygen-evolving complex of photosystem-2 - the role of tyrpsine-Z. *Biochemistry* **1992**, *31*, 4562−4573.
(57) Astashkin, A. V.; Mino, H.; Kawamori, A.; Ono, T. A. Pulsed EPR study of the S'(3) signal in the Ca^{2+}-depleted photosystem II. *Chem. Phys. Lett.* **1997**, *272*, 506−516.
(58) Cox, N.; Ho, F. M.; Pewnim, N.; Steffen, R.; Smith, P. J.; Havelius, K. G. V.; Hughes, J. L.; Debono, L.; Styring, S.; Krausz, E.; Pace, R. J. The S_1 split signal of photosystem II; a tyrosine-manganese coupled interaction. *Biochim. Biophys. Acta* **2009**, *1787*, 882−889.
(59) Havelius, K. G. V.; Su, J. H.; Feyziyev, Y.; Mamedov, F.; Styring, S. Spectral resolution of the split EPR signals induced by illumination at 5 K from the S_1, S_3, and S_0 states in photosystem II. *Biochemistry* **2006**, *45*, 9279−9290.
(60) Su, J. H.; Havelius, K. G. V.; Mamedov, F.; Ho, F. M.; Styring, S. Split EPR signals from photosystem II are modified by methanol, reflecting S state-dependent binding and alterations in the magnetic coupling in the $CaMn_4$ cluster. *Biochemistry* **2006**, *45*, 7617−7627.
(61) Pavlou, A.; Styring, S.; Mamedov, F. The S_1 to S_2 and S_2 to S_3 state transitions in plant photosystem II: relevance to the functional and structural heterogeneity of the water oxidizing complex. *Photosyn. Res.* **2024**, *162*, 401−411.
(62) Khangulov, S.; Sivaraja, M.; Barynin, V. V.; Dismukes, G. C. The dimanganese(III,IV) oxidation-state of catalase from *thermus thermophilus* electron nuclear double resonance analysis of water and protein ligands in the active site. *Biochemistry* **1993**, *32*, 4912−4924.
(63) Drosou, M.; Comas-Vila, G.; Neese, F.; Salvador, P.; Pantazis, D. A. Does Serial Femtosecond Crystallography Depict State-Specific Catalytic Intermediates of the Oxygen-Evolving Complex. *J. Am. Chem. Soc.* **2023**, *145*, 10604.
(64) Isobe, H.; Shoji, M.; Yamanaka, S.; Mino, H.; Umena, Y.; Kawakami, K.; Kamiya, N.; Shen, J. R.; Yamaguchi, K. Generalized approximate spin projection calculations of effective exchange integrals of the $CaMn_4O_5$ cluster in the S_1 and S_3 states of the oxygen evolving complex of photosystem II. *Phys. Chem. Chem. Phys.* **2014**, *16*, 11911−11923.
(65) Tamura, H.; Saito, K.; Nishio, S.; Ishikita, H. Electron-Transfer Route in the Early Oxidation States of the Mn_4CaO_5 Cluster in Photosystem II. *J. Phys. Chem. B* **2023**, *127*, 205−211.
(66) Suga, M.; Akita, F.; Hirata, K.; Ueno, G.; Murakami, H.; Nakajima, Y.; Shimizu, T.; Yamashita, K.; Yamamoto, M.; Ago, H.; Shen, J. R. Native structure of photosystem II at 1.95 A resolution viewed by femtosecond X-ray pulses. *Nature* **2015**, *517*, 99−103.
(67) Drosou, M.; Zahariou, G.; Pantazis, D. A. Orientational Jahn-Teller Isomerism in the Dark-Stable State of Nature's Water Oxidase. *Angew. Chem., Int. Ed. Engl.* **2021**, *60*, 13493−13499.
(68) Cox, N.; Rapatskiy, L.; Su, J. H.; Pantazis, D. A.; Sugiura, M.; Kulik, L.; Dorlet, P.; Rutherford, A. W.; Neese, F.; Boussac, A.; Lubitz, W.; Messinger, J. Effect of Ca^{2+}/Sr^{2+} substitution on the electronic structure of the oxygen-evolving complex of photosystem II: a combined multifrequency EPR, ^{55}Mn-ENDOR, and DFT study of the S_2 state. *J. Am. Chem. Soc.* **2011**, *133*, 3635−3648.
(69) Matsukawa, T.; Mino, H.; Yoneda, D.; Kawamori, A. Dual-mode EPR study of new signals from the S_3-state of oxygen-evolving complex in photosystem II. *Biochemistry* **1999**, *38*, 4072−4077.
(70) Leto, D. F.; Massie, A. A.; Colmer, H. E.; Jackson, T. A. X-Band Electron Paramagnetic Resonance Comparison of Mononuclear Mn-IV-oxo and Mn-IV-hydroxo Complexes and Quantum Chemical Investigation of Mn-IV Zero-Field Splitting. *Inorg. Chem.* **2016**, *55*, 3272−3282.
(71) Chen, H.; Dismukes, G. C.; Case, D. A. Resolving Ambiguous Protonation and Oxidation States in the Oxygen Evolving Complex of Photosystem II. *J. Phys. Chem. B* **2018**, *122*, 8654−8664.
(72) Kolling, D. R.; Cox, N.; Ananyev, G. M.; Pace, R. J.; Dismukes, G. C. What are the oxidation states of manganese required to catalyze photosynthetic water oxidation. *Biophys. J.* **2012**, *103*, 313−322.
(73) Kuntzleman, T.; Yocum, C. F. Reduction-induced inhibition and Mn(II) release from the photosystem II oxygen-evolving complex by hydroquinone or NH2OH are consistent with a Mn(lll)/Mn(III)/Mn(IV)/Mn(IV) oxidation state for the dark-adapted enzyme. *Biochemistry* **2005**, *44*, 2129−2142.
(74) Hillier, W.; Wydrzynski, T. Oxygen ligand exchange at metal sites -: implications for the O2 evolving mechanism of photosystem II. *Biochim. Biophys. Acta* **2001**, *1503*, 197−209.
(75) Pantazis, D. A. Evaluation of new low-valent computational models for the oxygen -evolving complex of photosystem II. *Chem. Phys. Lett.* **2020**, *753*, 137629.
(76) Ifuku, K. The PsbP and PsbQ family proteins in the photosynthetic machinery of chloroplasts. *Plant Phys. Biochem.* **2014**, *81*, 108−114.

https://doi.org/10.1021/acsphyschemau.5c00068
ACS Phys. Chem Au 2025, 5, 660−671